J MATER RES TECHNOL. 2019;8(2):2269–2279

Available online at www.sciencedirect.com

jmr&t Journal of Materials Research and Technology

www.jmrt.com.br

Original Article

On the microstructure effects when using electropulsing versus furnace treatments while drawing inox 308L

A.J. Sánchez Egea[a,*], J. Jorba Peiró[b], Javier Walter Signorelli[c], H.A. González Rojas[d], Diego Javier Celentano[a]

[a] Department of Mechanical and Metallurgical Engineering, Pontificia Universidad Católica de Chile, Av. Vicuña Mackenna 4860, Macul, Santiago de Chile, Chile

[b] Department of Materials Science and Metallurgical Engineering (EEBE), Universitat Politècnica de Catalunya, Eduard Maristany, 16, Barcelona, Spain

[c] Instituto de Física Rosario (IFIR-CONICET), Bv. 27 de febrero 210 bis, (2000), Rosario, Argentina

[d] Department of Mechanical Engineering (EPSEVG), Universitat Politècnica de Catalunya, Av. de Víctor Balaguer, 1, Vilanova i la Geltrú, Barcelona, Spain

ARTICLE INFO

Article history:
Received 17 December 2018
Accepted 29 March 2019
Available online 7 May 2019

Keywords:
Resistivity
Detwinning
Recrystallization
Calorimetry
Texture
Inox 308L

ABSTRACT

In the present work, microstructure and texture evolution in a commercial 308L stainless steel wire is assessed by comparing several electropulsing configurations and thermal annealing treatments performed during and after a single pass wire drawing process. In this context, the objective is to determine if the electropulsing brings significant differences on the material microstructure with respect to a conventional annealing treatment. To this end, electron backscattered diffraction was used to analyze the microstructure changes in all the studied cases. The results indicate that recrystallization and detwinning are drastically accelerated when in situ electropulsing treatment is applied in the specimen during its drawing. Moreover, electropulsing or large times of furnace treatments after the wire drawing are found to enhance the material conductivity compared to the in situ electropulsing treatment during the wire drawing. Finally, differential scanning calorimetry and material resistivity are performed to analyze the thermal events in a meso/micro scale. Accordingly, the bulk temperature for the electropulsed specimens is assumed to be much higher than the bulk temperature recorded at the surface of the specimen.

* *Corresponding author.*
E-mail: antonio.egea@ing.puc.cl (A. Sánchez Egea).

https://doi.org/10.1016/j.jmrt.2019.03.007

1. Introduction

Wire drawing is a metal forming process used for the reduction of the cross section in one or several steps to reach the desired wire diameter. Due to the cold deformation, the wire becomes harder, the tensile strength increases and the ductility decreases. During the reduction of the cross section with different drawing dies, the wire needs an annealing treatment to restore the plasticity, relief residual stresses and increase the ductility [1]. During this thermal treatment, temperature and time are crucial to achieve the proper material recrystallization for further redrawing. This recrystallization process brings microstructural alterations in metal alloys that change the mechanical properties. These microstructural changes are performed through different scenarios, like recrystallization mechanism, detwinning process or reorientation of crystallographic distribution (texture evolution), as investigated by Hull and Bacon [2]. In this sense, the phase transformations are commonly investigated when either a strain-induced or a thermal treatment are carried out with the aim to optimize this manufacturing process. Consequently, dislocations, twins and grain boundaries play a key role in these microstructural changes and, subsequently, in the mechanical properties of the material in service.

Electrically assisted manufacturing processes offer a potential solution to avoid time consumption of conventional annealing treatments between drawing steps. In particular, several experimental [3] and modeling [4] reviews about electropulsing treatments had shown a relevant efficiency of this manufacturing process compared with traditional metal forming processes. This novel treatment can modify the material microstructure and material texture with an ultra-fast annealing treatment, which is mainly attributed to the temperature variation in a macro and micro scale. Additionally, Kuang et al. [5] have shown that other effects could possibly have an influence on the grain boundaries orientation, when comparing metallurgical analysis of this novel technique with a conventional thermal treatment. Our previous results (Sánchez Egea et al. [6]) stated that a dynamic recrystallization process increases uneven grain size in the electrically assisted specimens by a fast rise of temperature. In particular, an unalike detwinning mechanism and a lower volume fraction of α-martensite were found when comparing conventional and electrically assisted specimens. Moreover, the electrically assisted specimen presented a detwinning process with a less density and different misorientation angle distribution in magnesium alloys [7]. Recently, Wang et al. [8] showed the influence of the electropulses on the twinning behavior during a micro tension tests. They mentioned that the electroplastic effect brought different twinning behavior in AZ31 alloy depending on the strain rate and the grain size. Additionally, Xu et al. [9] stated that the twins and grain boundaries distribution are reoriented when an electron flow is induced through the microstructure of the Ti–6Al–4V alloy. They stated that dynamic recrystallization brought a decrease of the grain size while an increase of the volume fraction of recrystallized grains. In particular, the primary contraction twins present higher number of fraction and Schmid factor, which are associated with an increase on the material formability.

Despite these promising results, further research in a micron and submicron scale is required to understand the mechanisms that modify these microstructure variations when an electron flow is induced through metallic alloys before, during and after plastic deformation. In this context, the primary interest is to determine not only if the electron flow promotes a particular preferential crystal orientation in the material microstructure, but also to understand how the twins and dislocations behave when electropulsing is combined with plastic deformation. If in a nearly future it is expected to use the electropulsing treatment in industrial applications, a thorough investigation of the microstructure and texture evolution of the metal alloys is crucial to comprehend the electroplastic effects while a plastic deformation is performed. In the present paper, microstructure and texture evolution in a 308L stainless steel wire is investigated by comparing electropulsing versus furnace treatments. To achieve that, several configurations of electropulsing and conventional thermal treatment are performed during and after a single pass wire drawing process. The objective is to determine if the electropulsing brings significant differences on the material microstructure with respect to a conventional annealed treatment. Therefore, the material hardness, microstructure changes, detwinning, resistivity, calorimetry and crystallographic texture are investigated to comprehend if the electropulsing can enhance the capabilities of wire drawing and, thus, can avoid the time consuming conventional annealing treatments.

2. Materials and methodology

A commercial wire of 308L stainless steel (0.03 wt% C, 19 wt% Cr, 9.7 wt% Ni, 0.45 wt% Si, 1.8 wt% Mn, 0.04 wt% P, 0.03 wt% S, and balance Fe) with a diameter of 1.60 mm, attained as a result of previous wire drawing steps, was analyzed in this investigation. The wire was then cold-drawn in a single pass with the largest reduction before cracking. The wire drawing tests were conducted in an Instron 4206 universal testing machine. The wire was drawn with a constant velocity of 0.5 m/min, while the cross sectional area reduction and the semi-angle of the conic die were kept to 15.6% and 6°, respectively. Fracture of the specimens was found when higher cross sectional area reductions were conducted. During the experiments powder soap was applied as a drawing lubricant and the drawing forces were measured with a load cell connected to the lower clamp of the tensile machine.

An in-house electropulsing generator was applied to discharge positive direction multiple pulses with the following features: RMS current density of 34.8 A/mm^2, pulse duration of 250 μs and frequency discharge of 142 Hz, according to our previous work [6]. An oscilloscope was equipped in the circuit for monitoring the electropulsing treatment. According to these electric parameters, the wire drawing velocity and the cross sectional area of the wire, the instantaneous bulk temperature recorded during the assisted experiments was 330 ± 8 °C. This temperature will be the reference to perform the conventional thermal treatments with different periods of time. A K-type thermocouple was used to measure the surface temperature variation for each test. The metallographic structure

was observed before and after the electropulsing treatment by a Nikon microscope (Optiphot-100). The grain size and twins distribution were analyzed with the electron backscatter diffraction (EBSD) module, using a Scanning Emission Electron (SEM) microscope, model: JEOL JSM 7001-F, with field emission electron configuration of 20 kV. The specimens were tilted at 70° and the working distance between the collector and specimen was 10 mm. Crystal orientation data were acquired over a cubic grid with a spacing of 0.2 μm. The MTEX toolbox was required for post-processing of the material microstructure and crystal misorientation [10].

Moreover, the material hardness variations on the specimens were measured with a durometer, Buelher model MicroMet 5114. A conventional oven (Carbolite, model ST-16) was utilized for the thermal treatments. The specimens were immersed into a melded lead bath to avoid oxidation and ensure the maximum temperature of 330 °C in the specimen during three time intervals of thermal treatment: 15, 150 and 1500 s. The thermal stability was measured with a Differential Scanning Calorimetry (DSC) model NETZSCH DSC 404F3. A thermal rate of 20 K/min was considered for these experiments starting from 100 °C to reach the temperature of 1400 °C. The temperature accuracy was set to ±1 °C according to the metal melting standards. The experimental sensitivity was about 0.08 μV/mW for temperatures around 100 °C. A preheating process was carried out to make sure the thermal homogeneity and Argon (Ar) gas was used to prevent oxidation. An alumina sample pan was used as crucible for the thermal analysis of 0.23 mg, whereas the sample weight average was 0.07 mg.

Finally, a four-wire resistance measurement technique was carried out to measure the bulk resistivity for each specimen. For that purpose, a digital multimeter (model: Keithey 2100) with 6½-digit measurement resolution was used. In order to increase the accuracy of the resistivity measurement at room temperature, several precautions were assumed: 200 mm length of the sample, temperature control (minimize Joule effect), clips for electrical connections and a ten number of measurements were done by increasing the current intensity through the wires. In this sense, the margin errors in the resistivity measurements were found to be around 0.1 nΩm. The microstructure changes were investigated in eight different wire drawing configurations using three specimens per configuration: as-received (B), conventional drawn (CD), electropulsing assisted drawn (EPD), conventional drawn and later electropulses (STC), electropulses induced to the as-received (PST) and three thermal treatments with time durations 15 s (TT-15s), 150 s (TT-150s) and 1500 s (TT-1500s) at a temperature of 330 °C.

3. Results

3.1. Material hardness

The material hardness of each configuration is recorded to denote how the different thermal treatments affect the studied specimens. Fig. 1 shows the material hardness of 10 measurements for each configuration along the specimen length. These measurements were taken from different specimens. The hardness values are achieved with a penetration force and time of 200 g and 15 s, respectively. The horizontal lines of the box plots represent the median, first and third quartile, the squares represent the average, the whiskers represent the tenth and ninetieth percentile and the crosses below and above the box plots represent the maximum and minimum sided values.

Three different groups are denoted from the results, the first one is represented by CD, TT-15s and TT-150s configurations which show the higher material hardness of about 375 Vickers on average. This high hardness value is attributed to the plastic deformation during the drawing process, since for the two thermal treated configurations the achieved temperature has not been enough to cause a thermal softening. Secondly, the B, STC, PST and TT-1500s configurations present quite similar material hardness within the range of 335–350 Vickers. Only the STC and TT-1500s configurations show slightly higher values due to the plastic deformation. However, the large time of thermal treatments and the electropulsing treatment have shown to decrease the material hardness to similar values than the as-received material (B). Finally, the EPD configuration presents the lowest hardness values, about 320 Vickers on average. Consequently, the electropulsing treatment applied in situ when the specimen is plastically deformed denoted higher effectiveness on decreasing the internal material stresses.

3.2. Material resistivity

After the wire drawing process, it is assumed that the material resistance has changed due to mainly the plastic deformation and temperature. Fig. 2 presents the material resistivity for each configuration and the margin error estimated with a confidence interval of 95% of probability.

As expected, the CD specimen increases its resistivity due to the increasing degree of plastic deformation in its microstructure compared with the as-received specimen. Despite that the EPD sample presents a decrease of resistivity compared with that of the CD sample, this resistivity is not comparable with the TTs due to the recrystallization process observed in the material microstructure. Regarding to the PST specimen, it shows a decrease of resistivity compared with the as-received material, which seems reasonable if the current has an effect of sorting/annihilating of the microstructure defects. The STC specimen exhibits a resistivity value much lower than those of the CD and EPD samples. Consequently, the electropulsing (fast thermal softening) applied after wire drawing seems to facilitate a decrease in the resistivity up to comparable values to those of the as-received specimen. However, the effect on resistivity of the STC sample is not comparable with that of the PST sample, despite of inducing the same electropulsing conditions, because of the plastic deformation suffered by STC during the drawing operation. In our previous research [6], a partial recrystallization process was recorded in the 308L metal alloy improving its material formability. Similar to the present study, the recrystallization processes were not fulfilled and, as a consequence, the as-received sample still shows lower values of resistivity compared with EPD and STC. Finally, the conventional thermal treatments with different times have shown to decrease

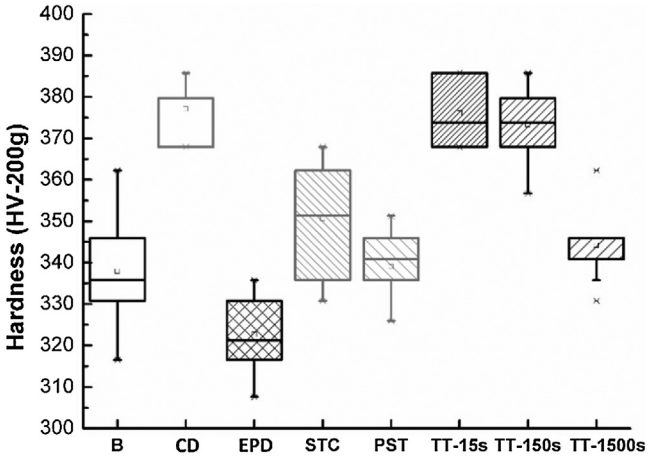

Fig. 1 – Material hardness measured along the sample length for each configuration.

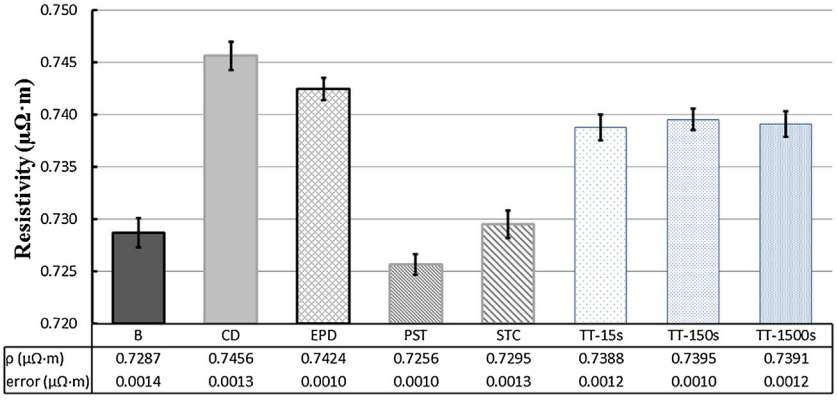

Fig. 2 – Measured material's resistivity by using a four-wire resistance method at room temperature.

the resistivity by 4% with respect to that of the CD sample. This change of resistivity is attributed to the thermal effects that help to rearrange the material microstructure. It is noticed that the PST and STC configurations have been much effective in reducing the material resistivity, suggesting that the electropulsing before and after the plastic deformation promote better results on the material conductivity compared with the in situ electropulses during the plastic deformation (EPD).

3.3. *Microstructure changes*

In order to quantitatively compare the microstructures changes, the Standard Test Methods for Determining Average Grain Size ASTM E112 have been followed to measure the grain size for each configuration. The grain size and area of the microstructure of each wire drawn specimen are measured. Also, the grain aspect ratio is estimated by dividing the grain size in the radial direction (perpendicular to the drawing direction) and axial direction (parallel drawing direction). Table 1 depicts the average grain sizes and grain aspect ratio for all the studied configurations. In general, the specimens seem to exhibit the trend in grain aspect ratio where the axial dimension is bigger than the radial dimension.

The average grain size of the EPD sample is much larger in both directions than that of the CD sample and the grain aspect ratio is diminished from 2.08 to 1.67. Consequently, the EPD specimen presents a more equiaxed grains than that of the CD specimen. On the contrary, the electropulsing treatment applied after drawing (STC) exhibits that the grain size is a little larger than that of the CD sample in both directions, showing also that the grain aspect ratio is the same. Furthermore, the grain aspect ratio tends to reduce when larger times of TT are applied on previously wire drawn specimens. Looking the electropulsing treatment applied on the as-received specimen (PST), it is showed that the grain size is bigger in both dimensions than that of the B sample, but the grain aspect ratio presents a similar value. The average of the grain area distributions for the different studied configurations are represented in Fig. 3. The histograms are obtained from the EBSD images with a misorientation angle threshold set to 5°.

Different grain area distributions are clearly found for the wire drawing process assisted with electropulsing (EPD) with respect to the samples treated with a furnace during 150 s and 1500 s. These results of the grain area distribution and the grain aspect ratio values suggest that a partial recrystallization process was achieved for the EDP and TT configurations, with no clear recrystallization evidence in the other configurations. For the EPD specimen, about half of the grains show an area of about or higher than 500 μm^2. For the TT specimen with 150 and 1500 s, only few grains show an area of about 500 μm^2. The

Table 1 – Grain dimensions of the microstructure recorded from the EBSD images.

Grain metrics	B	CD	EPD	PST	STC	TT-15s	TT-150s	TT-1500s
Radial direction [μm]	7.01	7.71	13.33	10.18	7.82	7.71	8.57	8.71
Axial direction [μm]	11.07	16.01	22.22	16.08	16.27	17.14	16.55	16.84
Grain aspect ratio	1.58	2.08	1.67	1.57	2.08	2.11	1.93	1.87

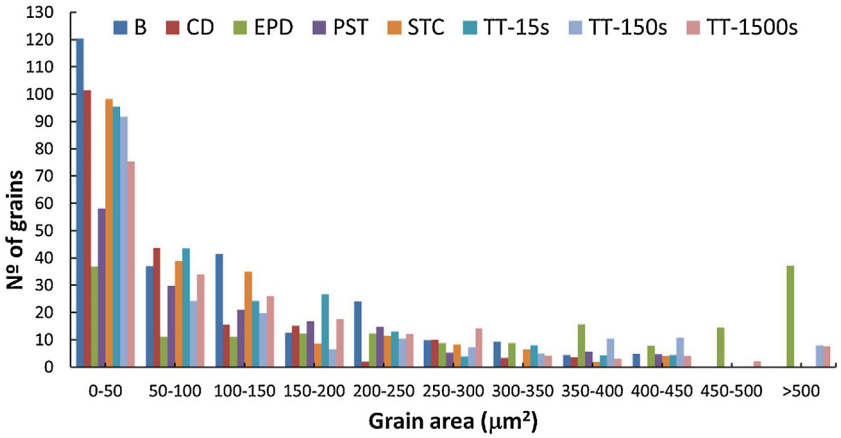

Fig. 3 – Average grain area distributions of the different configurations. A standard grain recognition procedure was used, with a misorientation angle threshold set to 5°.

Table 2 – Local misorientation metrics (GOS, KAM, and GAM) for the different configuration.

Sample configuration	Misorientation metrics (average values)		
	GOS	KAM	GAM
B	1.69	1.08	3.41
CD	1.52	1.25	2.63
EPD	1.30	1.01	4.53
PST	1.82	1.17	4.69
STC	1.31	1.27	2.05
TT-15s	1.81	1.32	5.19
TT-150s	1.55	1.10	4.67
TT-1500s	1.77	1.36	6.01

B and CD specimens present an average grain area of about 100 μm^2 with a lot of twins, in particular for the as-received specimen which came, as already mentioned, from previous wire drawing steps. Moreover, local misorientation metrics are estimated to investigate to effect of the temperature in the microstructure changes. Consequently, Table 2 exhibits some local misorientation metrics described by Wright et al. [11], i.e. Grain Orientation Spread (GOS), Kernel Average Misorientation (KAM) and Grain Average Misorientation (GAM). In this sense, it is possible to describe the microstructure changes of each studied configuration and indirectly the local metallographic state of the grain boundaries [12] and grains [13]. Accordingly, several authors agreed that in aluminum [14] and titanium [15], the dynamic recrystallized grains exhibit low GOS values of ~1–2° and created nuclei below 1°.

In our case, the misorientation metrics show that the drawing process in situ assisted with electropulsing (EPD) presents the lowest values of GOS and KAM compatible with the state of dynamic recrystallization. Observing the GOS histogram (see in appendix material), it is possible to appreciate that the fraction of grains with a GOS value below than 1° is approximately 50% of the data. In particular, the most frequent results are found between 0.6° and 0.8°, where the histograms were made using a bin of 0.2°. The low values of KAM could be explained by the low density of grain limits and comparatively low number of wide non-deformed twins; see Fig. 4a. Consequently, an evident recrystallization process that has made to grow the grain and reduce the aspect ratio; see Table 1.

On the other hand, the values of GOS and KAM in the CD configuration are higher than that of the EPD configuration, as expected due to the high density of high and low angle grain limits, and deformed twins; see Fig. 4b. In addition, the values of GOS and KAM for the STC (electropulses after conventional drawing) configuration are similar to those of the EPD and CD configurations, respectively. In this case, the GOS histogram (see in appendix material) shows that the fraction of grains with GOS of 1° is approximately 40%, which is a value compatible with a recrystallization. However, this recrystallization is limited, because an important part of previous material has not been rearranged and still retains an important density of grain limits and twins; see Fig. 4b. This would explain that the value of KAM is similar to the CD configuration. Furthermore, the TT-150s and TT-1500s show GOS distribution similar to that of the EPD configuration, where the fraction of grains with values below 1° are about 30% for the TT configurations and 34% for the EPD configuration. In both configurations, the frequent range of values are within 0.8° and 1.0°, but the GOS and KAM values are higher than EPD configuration. These results can be explained in the same way for the STC configuration, but considering that recrystallization is more incipient in the EPD configuration than in the STC configuration. Further information of the GOS, KAM and

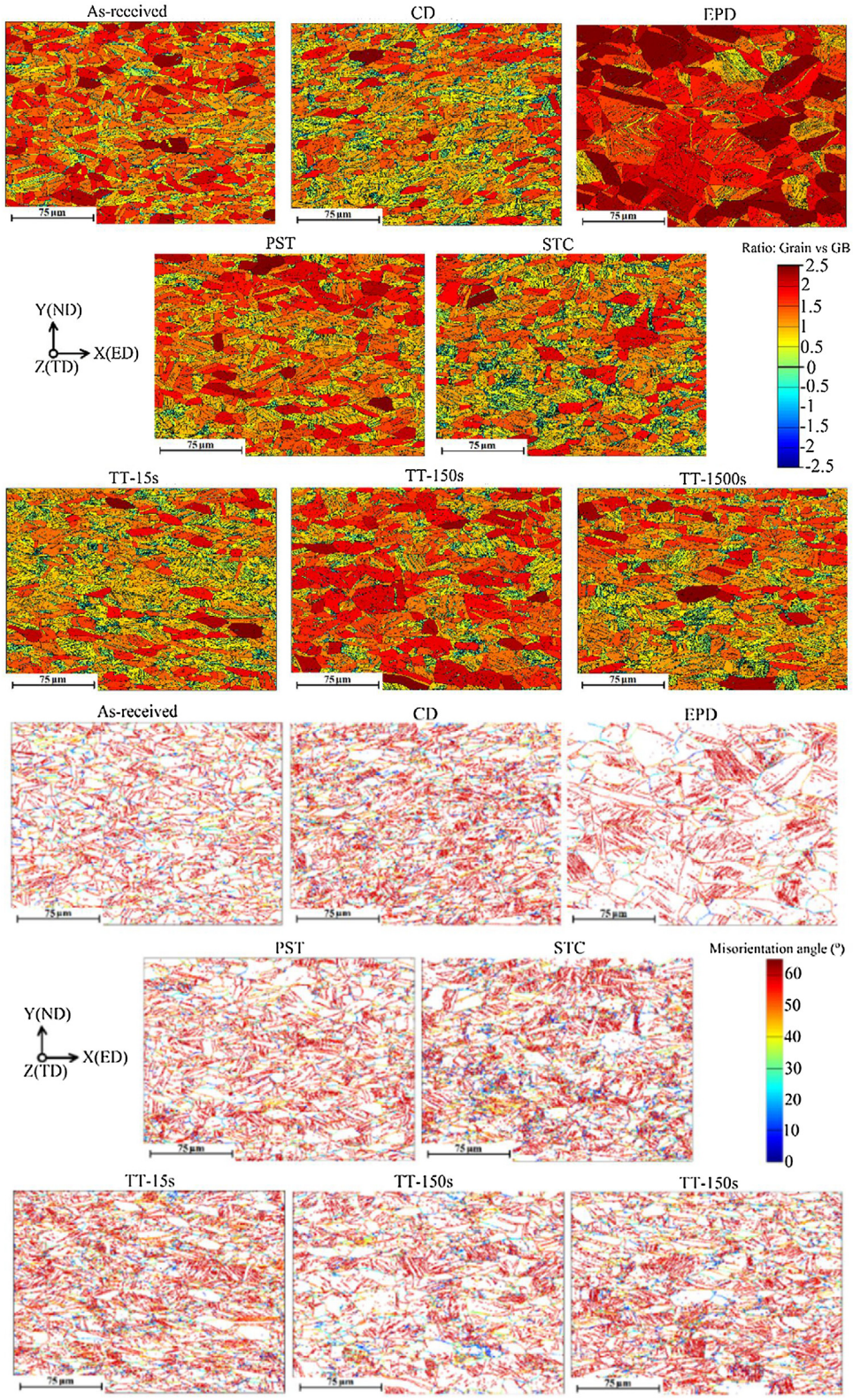

Fig. 4 – (a) Ratio between grain size and grain boundaries of the different configurations. (b) High and low-angle grain boundaries distribution in the microstructure of the different configurations.

GAM histograms can be found in the supplementary material of this manuscript.

3.4. *Twins and grain boundary*

Fig. 4a outlines the ratios between grain size and grain boundaries for the different specimens. The direction normal to the analyzed surface of the samples is denoted as (ND) and corresponds to the center of wire, while for the other two planes are named as transverse direction (TD) and drawing direction (ED). Fig. 4b exhibits low-angle grain boundary distributions within the grain with dark colors and high-angle grain boundaries with light colors, as shown in the misorientation color palette.

Initially, the B, CD and TT-15s specimens show a microstructure with a shape elongated along the drawing direction and with a large number of twins, which are clear factors of a severely distorted microstructure. On the contrary, the EPD specimen shows a microstructure with almost equiaxed big grains with low presence of twins (detwinning). This type of microstructure is typical of an annealed specimen, where the material stresses from a previous plastic deformation have been eliminated. In previous works, a detwinning process was also found in different electrically assisted forming processes: drawing stainless steel [16] and V-bending magnesium alloy [17]. Apart from that, several reports have stated that an electric field enhances the dynamic recrystallization tending to coarsening the grain size depending on the metallic alloy and the applied electric energy [18,19]. Accordingly, it is assumed that the electropulsing treatment can induce a more or less extensive recrystallization in all configurations and their effects are consistent with the hardness values shown in Fig. 1. The decrease of material hardness was also reported by Zhou et al. [20] when Ti6Al4V was electrically assisted during a cold drawing process. This recrystallization is obtained from the accumulation of dislocations at the grains and subgrain boundaries which, ultimately, turn out into high-angle boundaries when a certain level of energy is stored in those regions. The reduction of the twin density and the growth of grain are also appreciable in the STC and TT samples, when they are compared with those of the CD sample, but clearly smaller than those of EPD sample.

3.5. *Microstructure orientation*

The Inverse Pole Figures (IPFs) for the (111) and (220) directions together with the (111) and (220) Pole Figures (PFs) of the FCC structure of each configuration are presented in Figs. 5 and 6, respectively. In both cases, the same contour levels have been used in order to highlight the similarities and differences for all configurations. These textures are treated with MTEX package (http://mtex-toolbox.github.io/) assuming a half-width of 3.5° and a resolution of 1.5° for the Orientation Distribution Function (ODF) evaluation.

Plastic deformation generates preferred crystallographic orientations characterized by specific ideal orientations and fibers. Consequently, the volume fraction and intensity of these texture components are key parameters to distil out subtle variations between textures which in our case describe the plastic deformation and the thermal softening achieved in each specimen. The IPF for the as-received material (B) presents a preferred orientation toward a direction between [001] and [011] for the plane (220) and an incipient orientation to [001] in the plane (111). However, in the CD configuration, the preferred crystal orientations have rotated and present the highest intensity toward the directions [001] and [011] for the planes figures (111) and (220), respectively. In both samples, the PFs show a well-defined distribution of intensities for the planes (111) and (220). On the other hand, the thermal treated samples after conventional drawing (TT-150s and TT-1500s) exhibit an IPF with remaining preferential orientation in [001] for (111) and a still well-defined distribution of intensities in the planes (111) and (220). Compared with the CD configuration, the TT-1500 case shows a degree of blurring that would correspond to an accommodation of the crystals different from the preferential distribution orientation of the analyzed grains, which is compatible with a partial recrystallization of the material. As expected, this blurring is more evident in the PST configuration than in the as-received condition due to the extra thermal effect through electropulsing. The blurring is once again apparent when comparing the CD configuration with the STC case, also associated with the electropulsing assisted after the wire drawing process. Moreover, the lowest degree of intensity is displayed for the EPD configuration plus an evident reorientation to from the [011] to $[1\bar{1}\bar{1}]$ for the plane (220). According to these evidences, the electropulsing treatment used for the different configurations facilitate the crystal accommodation and the reorientation of the crystal orientation different from the preferential crystal distribution, as shown in Figs. 5 and 6.

4. Discussion

According to the aforementioned results, conventional thermal treatments used to promote a thermal softening in the material have shown to influence the material microstructure and metallography properties in a different manner than that observed in the electropulsing assisted specimens. Despite that the specimens affected with longer time of thermal treatment show a higher grain size and lower density of grain boundaries, the results are not comparable with the microstructure changes found when inducing electropulses during the plastic deformation. For this reason, it is thought that the achieved temperature when inducing the electropulses in the meso/micro scale is much higher than the bulk temperature recorded at the surface of the specimen. In order to prove this fact, further analysis of material resistivity and differential scanning calorimetry (DSC) were carried out for supporting the discussion.

The resistivity of a material depends on the material itself and its crystalline structure, the temperature and the degree of plastic deformation of the material. Consequently, it is assumed that the resistivity results found for the CD and TT configurations cannot explain the result obtained for the STC sample. Accordingly, additional experiments have been carried out to applied different maximum bulk temperatures (210 °C, 240 °C, 330 °C and 500 °C) during a constant time of 15 s in the conventional wire drawn samples (CD). These samples have been immersed in baths of oil, lead or melded salts

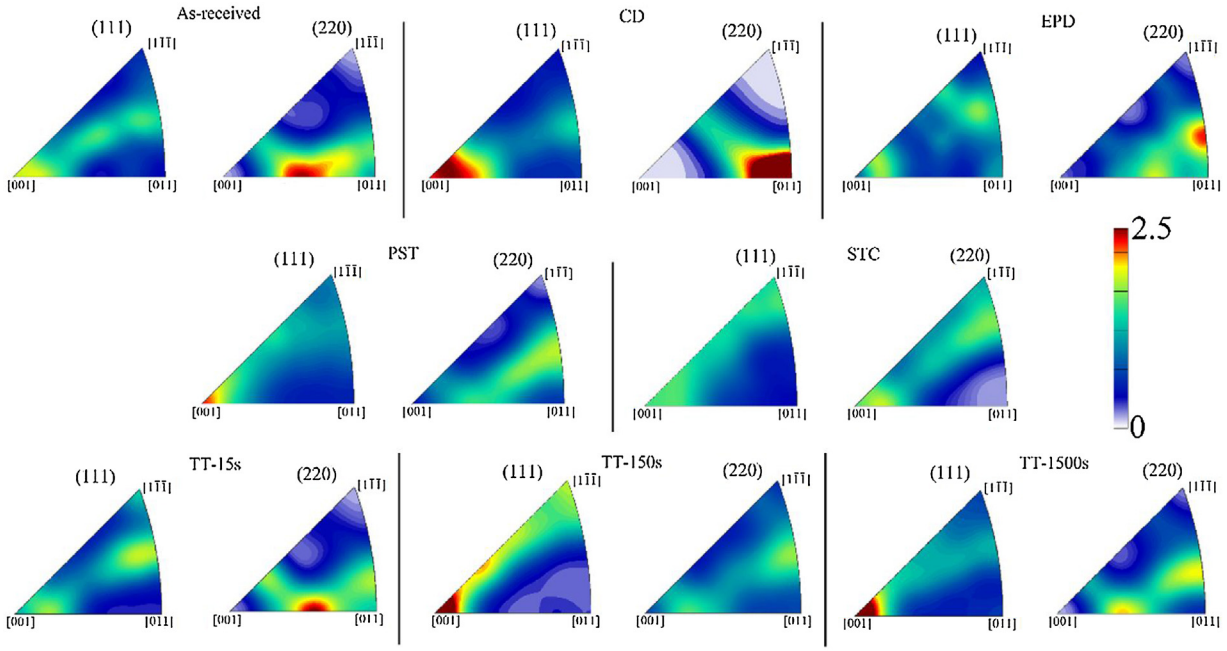

Fig. 5 – IPFs for the (111) and (220) directions for the different configurations.

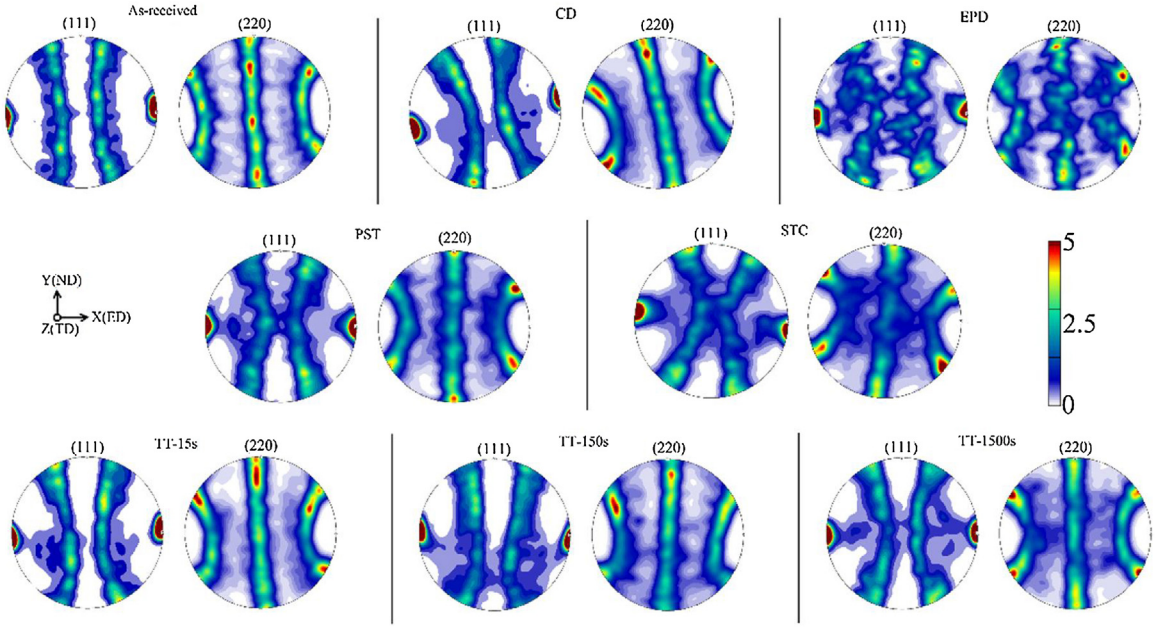

Fig. 6 – (111) and (220) PFs for the different configurations.

depending on the temperature to prevent oxidation. Fig. 7 shows the resistivity measures for different temperatures and type of thermal source that have been carried out under the same conditions than those of Fig. 2.

A decrease of the material resistivity is observed when the temperature of the thermal treatment increases. This result is consistent when the as-received specimen is plastically deformed (CD) and reorders its microstructure more widely when the temperature increases. However, the resistivity of the STC sample is smaller than the resistivity of the sample with a treatment at 500 °C during the same time of heat treatment. This would be possible if the temperature in a micro/meso scale had been much higher (hot-spots) than the one measured on the surface of the sample when the manufacturing process was assisted with electropulses. In addition, these hot-spots would have been generated in the areas of the material where there is a greater concentration of defects and/or voids in the lattice. Besides, these areas seem to initiate the reorganization processes of the deformed network. Furthermore, comparing the STC and PST samples, it

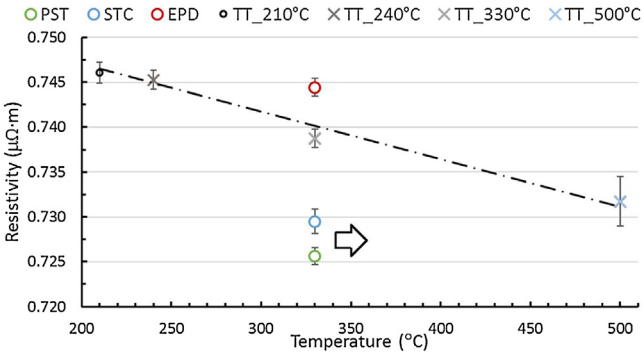

Fig. 7 – The material's resistivity according to the maximum achieved temperature and thermal source during a thermal treatment of 15 s.

is noted that the specimen with a higher accumulated plastic strain presents a higher resistivity, despite the fact that a higher current density was induced through the specimen due to its lower cross sectional area. Also, the value of the local temperature cannot be extrapolated using the same previous trend, because the degree of previous plastic deformation of the as-received material is smaller than that of the CD configuration. Additionally, the increase of the local temperature can exceed the maximum temperature, which allows the formation of α-martensite by transformation induced by plasticity (TRIP) of the austenite, as stated by Weiss et al. [21]. In this sense, it can be explained why the α-martensite is not formed when electropulsing is applied in situ during wire drawing (EPD), whereas α-martensite is formed during a conventional wire drawing (CD) at room temperature [6].

Nevertheless, this increase of the local temperature cannot explain why the resistivity in the EPD sample is in the same order than that of the CD sample and much higher than those samples with any applied thermal treatment. Only previous results can explain that change of resistivity which are associated to the higher grain size and lower density of low-angle grain boundaries. In this sense, Fig. 8 exhibits the DSC analysis of the B, CD and EPD samples with the aim of recording the thermal events that can occur during the experiment.

The results of DSC of the B and CD samples exhibit a similar thermal behavior, clearly showing in both cases endothermic peaks where, at the same temperature ranges, the EPD configuration presents a different trend without clear endothermic peaks compared with the aforementioned configurations. The first endothermic peak occurs around 560 °C which corresponds to the transformation of α-martensite, present in B and CD samples and formed during plastic deformation, into phase gamma as was also rigorously reported by Shuro et al. [22] when investigated the microstructural changes of 304 stainless steel under different isothermal thermal treatments. However, this endothermic peak is not appreciable in the EPD sample, which allows us to assume that there was not a formation of α-martensite by TRIP or that such formation has been attenuated during the electropulsing assisted process, as observed and discussed in our previous work [6]. Then, for the B and CD specimens, a second endothermic peak is observed at around 800 °C. This peak could be attributed to the dissolution of the carbides and nitrides present in the austenite matrix; similar results were reported in an austenitic 304 stainless steel by Petrovič et al. [23]. In accordance with the aforementioned peak, the EPD sample does not exhibits this second endothermic peak. Accordingly, Lu et al. (2014) stated that the electropulsing treatment promoted fast dilution of microstructural defects, inclusions and voids [24]. The dissolution of these microstructural defects could be attributed to a fast rise of the temperature in a localized region (hot-spot) due to the change on the material resistivity which, as a consequence, leads to high tension/compression stresses localized in these microstructural regions. These hot-spot are difficult to measure with conventional measurement devices. For that reason, the DSC and the recrystallization observation provide more information about temperature occurrence when inducing an electric field in the specimens. Additionally, the interaction of electrons with the dislocation promotes the dislocation mobility toward the grain

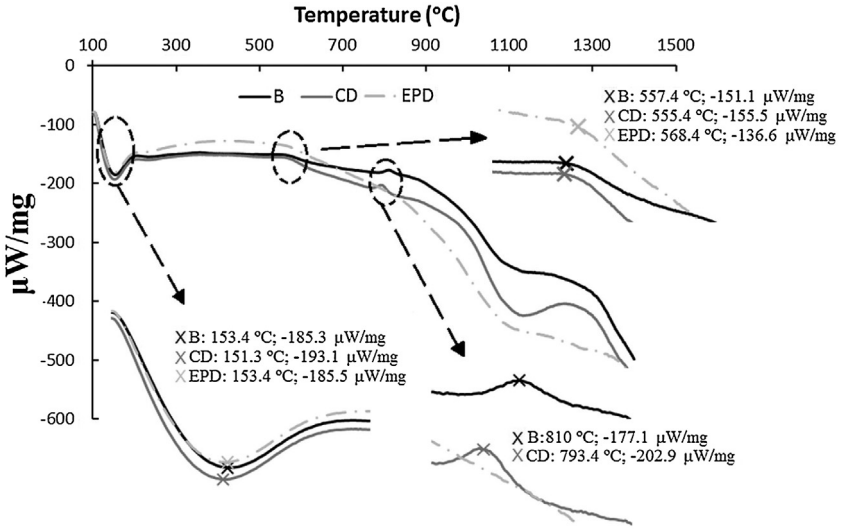

Fig. 8 – Differential scanning calorimetry of melting curves of B, CD and EPD specimens when using a heating rate of 20 K/min and a static Argon atmosphere.

boundaries and, at some points, the nucleation of new larger grains by dissolving small grains, precipitates and material impurities. The recrystallization process has an influence on the crystal orientation and improves the strain accommodation and, consequently, increases the formability of the specimen for future drawing steps. Besides, the detwinning process can be attributed to the annihilation of dislocation when an electric current is applied during plastic deformation because the ultra-fast temperature rises beyond the annealing temperature. Nevertheless, much research is needed to prove how and which mechanisms occur when an electric field (pulsed or not) is applied through different metallic alloys under plastic deformation.

5. Conclusions

The present study has investigated the microstructure changes of a 308L stainless steel when applying different electropulsing and furnace treatments in a single pass cold-drawing process. The main aspects found along the manuscript can be summarized as:

1. A decrease of the material hardness is attributed to the different thermal treatments. In particular, the electropulsing treatment presents a higher influence in reducing the material hardness when comparing with larger thermal treatments. Nevertheless, the material resistivity decreases when the thermal events are presented after the plastic deformation of the specimen.
2. The crystallographic texture shows that the in situ electropulsing while performing plastic deformation enhances the recrystallization, detwinning process and accommodation of the microstructure with a rotation of the fiber orientation distribution compared with the other thermal treatments.
3. The results of differential scanning calorimetry and material's resistivity denoted that higher temperature during the recrystallization process occurred when electropulsing is utilized, despite that the measurement devices have not recorded such high temperatures. Therefore, the electric field promotes an ultra-fast annealing treatment that rapidly transforms the microstructure of the specimen and facilitates the crystal reorientation. In particular, the electropulses inhibit the formation of α-martensite and, due to the fast thermal treatment, the initial α-martensite seems to be entirely transformed into austenite.

Conflicts of interest

All the authors who sign this manuscript do not have any conflict of interest to declare. Furthermore, the corresponding author certifies that this work has not been submitted to or published in any other journal.

Acknowledgements

This work is supported by the National Council for Scientific and Technological Development of Chile (Fondecyt projects 3180006 and 1180591). The authors want to thanks to Isaac López Insa for his valuable support using the electron backscatter diffraction equipment.

Appendix A. Supplementary data

Supplementary data associated with this article can be found, in the online version, at doi:10.1016/j.jmrt.2019.03.007.

REFERENCES

[1] Hull D, Bacon DJ. Introduction to dislocations. 5th ed. Elsevier Ltd.; 2011.
[2] Nguyen-Tran HD, Oh HS, Hong ST, Han H, Cao J, Ahn SH, et al. A review of electrically-assisted manufacturing. Int J Precis Eng Manuf-Green Technol 2014;2:365–76.
[3] Ruszkiewicz BJ, Grimm T, Ragai I, Mears L, Roth JT. A review of electrically-assisted manufacturing with emphasis on modeling and understanding of the electroplastic effect. J Manuf Sci Eng 2017;139(11), 110801/1–110801/15.
[4] Kuang J, Du XP, Li XH, Yang YY, Luo AA, Tang G. Athermal influence of pulsed electric current on the twinning behavior of Mg–3Al–1Zn alloy during rolling. Scr Mater 2015;114:151–5.
[5] Sánchez Egea AJ, González Rojas HA, Celentano DJ, Jorba Peiró J. Mechanical and metallurgical changes on 308L wires drawn by electropulses. Mater Des 2016;90:1159–69.
[6] Kuang J, Li X, Zhang R, Ye Y, Luo AA, Tang G. Enhanced rollability of Mg–3Al–1Zn alloy by pulsed electric current: a comparative study. Mater Des 2016;100:204–16.
[7] Wang X, Xu J, Shan D, Guo B, Cao J. Modeling of thermal and mechanical behavior of a magnesium alloy AZ31 during electrically-assisted micro-tension. Int J Plasticity 2016;85:230–57.
[8] Ye XX, Tse ZTH, Tang GY, Song GL. Effect of electroplastic rolling on deformability, mechanical property and microstructure evolution of Ti–6Al–4V alloy strip. Mat Charact 2014;98:147–61.
[9] Hielscher R, Schaeben H. A novel pole figure inversion method: specification of the MTEX algorithm. J Appl Cryst 2008;41:1024–103.
[10] Wright SI, Nowell MM, Field DP. A review of strain analysis using electron backscatter diffraction. Microsc Microanal 2011;17:316–29.
[11] Mishra SK, Pant P, Narasimhan K, Rollett AD, Samajdar I. On the widths of orientation gradient zones adjacent to grain boundaries. Scr Mater 2009;61(3):273–6.
[12] Thomas I, Zaefferer S, Friedel F, Raabe D. High-resolution EBSD investigation of deformed and partially recrystallized IF steel. Adv Eng Mater 2003;5:566–70.
[13] Alvi MH, Cheong S, Weiland H, Rollett AD, Recrystallization. Texture development in hot rolled 1050 aluminum. Mater Sci Forum 2004;467:357–62.
[14] Mandal S, Mishra SK, Kumar A, Samajdar I, Sivaprasad PV, Jayakumar T, et al. Evolution and characterization of dynamically recrystallized microstructure in a titanium-modified austenitic stainless steel using ultrasonic and EBSD techniques. Philos Mag 2008;88(6):883–97.
[15] Sánchez Egea AJ, González Rojas HA, Celentano DJ, Jorba Peiró J, Cao J. Thermomechanical analysis of an

electrically-assisted wire drawing process. J Manuf Sci Eng 2017;139(11), 111017/1–111017/7.
[16] Xie HY, Wang Q, Liu K, Peng F, Dong XH, Wang J. Investigation of influence of direct-current pulses on springback during V-bending of AZ31B magnesium alloy sheet. J Mater Process Technol 2015;219:321–7.
[17] Li XP, Li XH, Zhu J, Ye XX, Tang G. Microstructure and texture evolution of cold-rolled Mg–3Al–1Zn alloy by electropulse treatment stimulating recrystallization. Scr Mater 2016;112:23–7.
[18] Fan R, Magargee J, Hu P, Cao J. Influence of grain size and grain boundaries on the thermal and mechanical behavior of 70/30 brass under electrically-assisted deformation. Mater Sci Eng A 2013;574(1):218–25.
[19] Zhou Y, Chen GQ, Fu XS, Zhou WL. Effect of electropulsing on deformation behavior of Ti–6Al–4V alloy during cold drawing. Trans Nonferrous Met Soc China 2014;24(4):1012–21.
[20] Weiss A, Gutte H, Scheller PR. Deformation induced martensite formation and its effect on transformation induced plasticity (TRIP). Steel Res Int 2006;77: 727–32.
[21] Shuro I, Umemoto M, Todaka Y, Kuo HH, Wang H. Anomalous property evolution during annealing in HPTed SUS 304 austenitic stainless steel. Mater Sci Forum 2011;667–669:589–92.
[22] Petrovic DS, Klancnik G, Pirnat M, Medved J. Differential scanning calorimetry study of the solidification sequence of austenitic stainless steel. J Therm Anal Calorim 2011;105:251–7.
[23] Lu WL, Zhang XF, Qin RS. Stability of precipitates under electropulsing in 316L stainless steel. Mater Sci Technol 2014;31(13A):1530–5.
[24] Wang X, Sánchez Egea AJ, Xu J, Meng X, Wang Z, Shan D, et al. Current-induced ductility enhancement of a magnesium alloy AZ31 in uniaxial micro-tension below 373 K. Materials 2019;12(111):1–12.